International Journal of Solids and Structures 94–95 (2016) 112–124

Contents lists available at ScienceDirect

International Journal of Solids and Structures

journal homepage: www.elsevier.com/locate/ijsolstr

2D mesoscale model for concrete based on the use of interface element with a high aspect ratio

Eduardo A. Rodrigues[a], Osvaldo L. Manzoli[b,*], Luís A.G. Bitencourt Jr.[a], Túlio N. Bittencourt[a]

[a] University of São Paulo, Av. Prof. Luciano Gualberto, Trav. 3 n. 380, CEP 05508-010 São Paulo, SP, Brazil
[b] São Paulo State University, UNESP/Bauru, Av. Eng. Luiz Edmundo C. Coube 14-01, CEP 17033-360 Bauru, SP, Brazil

ARTICLE INFO

Article history:
Received 1 October 2015
Revised 7 April 2016
Available online 12 May 2016

Keywords:
2D mesoscale analysis
Interfacial transition zone
Interface solid finite elements
Tension damage model
Concrete crack analysis

ABSTRACT

The mesostructure of concrete plays a very important role in the process of initiation and propagation of cracks. Microcracks tend to start in the Interfacial Transition Zone (ITZ) and propagate toward the mortar matrix until a macrocrack formation. Seeking to better understand the influence of the concrete mesoscopic structure, translated macroscopically in the form of loss of stiffness and energy dissipation, this work proposes a 2D mesoscale model in which the concrete is modeled as a heterogeneous three-phase material composed of coarse aggregates, mortar matrix and ITZ. The coarse aggregates are generated from a grading curve and placed into the mortar matrix randomly. Interface solid finite elements with a high aspect ratio are used to represent the ITZ and the crack process based on a mesh fragmentation technique. These interface elements present the same kinematics as the Continuum Strong Discontinuity Approach (CSDA), which allows the use of a continuum constitutive relation to describe their behavior. Thus, an appropriate continuum tension damage model is adopted to describe the complex nonlinear behavior of concrete due to the crack phenomenon. Initially, the proposed mesoscale approach is applied in uniaxial tensile tests to study the influence of the size, volume and distribution of the coarse aggregates within the mortar matrix. Then, three-point bending beams are simulated in mesoscale and the results compared with the experimental ones. The results showed that the proposed 2D mesoscale model presents the same kinds of characteristics that real 3D concrete shows, considering the effects of the mesostructure constituents.

1. Introduction

Concrete is a composite material made of coarse aggregate, sand (fine aggregate), cement and water. Nowadays, some additives are also included in the mixture. Therefore, concrete presents a highly heterogeneous microstructure, which leads to a complex structural behavior and cracking process, even for a simple external load condition.

As is well known, the mesostructure affects the macroscopic response of concrete and its internal structure plays a very important role in the process of initiation and propagation of cracks. Hence, numerical models in which concrete is assumed to be a homogeneous material are insufficient to rigorously establish the cause-effect link between the geometrical characteristics and physical properties with the corresponding macroscopic response (López et al., 2008).

Due to the recognized great influence of the internal structure on the mechanical behavior of heterogeneous materials, allied to the increased computational resources available nowadays, many numerical models have been proposed to study the concrete material at a mesoscopic level. Several models have been developed based on lattice models (Grassl and Jirásek, 2010; Schlangen and Garboczi, 1997; Schlangen and van Mier, 1992), in which the material is represented by a discrete system of structural elements (simple truss or beam elements) conveniently positioned, allowing for the assignment of different mechanical properties for elements failing in the mortar matrix, aggregates or ITZs. Other approaches have been based on particle models (Bolander Jr. and Saito, 1998; Cusatis et al., 2006; 2011; D'Addetta and Ramm, 2006; Zubelewicz and Bažant, 1987). From the numerical analysis point of view, these models are similar to the lattice models, also involving a discrete system of structural elements, but they are computationally more efficient due to the reduced number of unknowns. However,

* Corresponding author. Tel.: +55 11 31036000.
E-mail address: omanzoli@feb.unesp.br, oslmanzoli@gmail.com (O.L. Manzoli).

http://dx.doi.org/10.1016/j.ijsolstr.2016.05.004

the calibration of the parameters that describe the interaction between particles is a very difficult task. Continuum FEM models, characterized by the explicit representation of the mesoscopic constituents, have also been proposed (Häfner et al., 2006; Unger and Eckardt, 2011; Wang et al., 1999; Wriggers and Moftah, 2006). In these models, when the goals of the research are focused on the fracture process, discontinuities are introduced to the problem, using for example, special elements, such as zero-thickness interface elements (Caballero et al., 2007; 2006; Carol et al., 2001; López et al., 2008), or finite elements for capturing strong discontinuities by means of elemental (E-FEM) (Oliver et al., 2015; Roubin et al., 2015) or nodal enrichments (X-FEM) (Du et al., 2014).

In this paper, a 2D mesoscale model for concrete based on a continuum FEM approach is proposed. The development of this model involves two important tasks: generation of coarse aggregates and discretization of the created mesoscopic model in 2D finite elements (FEs).

Regarding the generation of coarse aggregates, the existing algorithms commonly take into account the shape, volume fraction and distribution of the particles within the sample. The shape depends on the aggregate type and, according to Wang et al. (1999), a rounded shape can be used for gravel aggregates while the geometry of crushed stone aggregates can be approximated by an angular shape. For the sake of simplicity, regular geometries, such as circular and elliptical shapes, are widely used (Bazant et al., 1990; Eliáš and Stang, 2012; Grassl et al., 2012; Grassl and Pearce, 2010; Leite et al., 2004; Mier and Vliet, 2003; Wang et al., 2015). Other researchers have also adopted arbitrary polygonal shapes (López et al., 2008; Wang et al., 1999). Kim and Al-Rub (2011) have investigated five different types of aggregate shapes in order to study the influence of the shape on the material behavior. Regarding the aggregate size distribution, two techniques are often used: grading curves and sieve analysis. Most researchers use the Fuller curve when a grading curve is adopted (Bazant et al., 1990; Carpinteri et al., 2004; Eliáš and Stang, 2012; Lilliu and van Mier, 2003; Schlangen and van Mier, 1992; Wittmann et al., 1993). Lastly, the aggregates are placed within the sample by means of several techniques, such as: take-and-place method (Häfner et al., 2006; Wriggers and Moftah, 2006); divide-and-fill method (De Schutter and Taerwe, 1993); Voronoi/Delaunay tessellations (Caballero et al., 2006; Niknezhad et al., 2015); stochastic-heuristic algorithm (Leite et al., 2004) and random particle drop method (Mier and Vliet, 2003). More recently, image processing techniques, such as scanning electron micrograph (Schlangen and Garboczi, 1997) or X-ray computed tomography (Garboczi, 2002; Huang et al., 2015; de Wolski et al., 2014) have been applied in order to obtain a more realistic representation of the shape and distribution of the particles.

The representation of the ITZ is the main challenge during the FE mesh generation process. In addition, the application of an appropriate strategy is essential due to the great influence of this region on the initiation of cracks in concrete. As pointed out by Monteiro et al. (1985), this region presents a very small thickness, which requires a fine mesh along the ITZ. The so-called aligned mesh approaches, in which the ITZ are explicitly represented, have been used by several authors (Wang et al., 1999; Wittmann et al., 1993; Wriggers and Moftah, 2006).

In this work an alternative model for modeling the concrete behavior using a mesoscale approach is proposed. The concrete is considered a three-phase material consisting of coarse aggregates, mortar matrix, and ITZ. The main novelty of the approach proposed is the use of standard low-order solid finite elements with a high aspect ratio, developed recently by Manzoli et al. (2012), to represent the ITZ and propagation through the mortar matrix by means of a mesh fragmentation technique (Manzoli et al., 2016). These elements are able to represent discontinuities by employing an appropriate continuum constitutive model, as can be seen in the recent successful applications for modeling of formation and propagation of crack networks induced by shrinkage in drying soils (Sánchez et al., 2014), cracks in quasi-brittle materials (Manzoli et al., 2016), as well as for modeling of bond slip behavior of reinforcing bars embedded in concrete (Rodrigues et al., 2015). In this work, the behavior of these elements (i.e. crack initiation and propagation) is described by a tension damage model. Finally, this constitutive model is integrated using an implicit-explicit (IMPL-EX) integration scheme to avoid problems of convergence during the analysis, commonly found in problems involving multiple cracks (Oliver et al., 2006; 2008). In order to generate and place the coarse aggregates into the mortar matrix, an efficient method based on Monte Carlo's simulation is employed. Thus, a grading curve is used during the generation of aggregates, which are placed into the mortar matrix randomly, so that no intersection between aggregates is allowed, as proposed by Wriggers and Moftah (2006). Moreover, for the sake of simplicity, regular geometry (octagon) for the coarse aggregates was chosen, since the intention was only to describe the new strategy developed for modeling concrete using a mesoscale approach.

The remainder of this paper is outlined as follows. In Section 2, the proposed mesoscale model for concrete is detailed. Attention is given to the strategy used for modeling the coarse aggregates and the presentation of the mesh fragmentation technique. The formulation of the interface solid finite element and the continuum tension damage model used to describe its behavior are described in Sections 3 and 4, respectively. In Section 5, numerical examples to validate the technique are performed. Finally, the main conclusions are drawn in Section 6.

2. Proposed mesoscale model for concrete

In the proposed mesoscale model for concrete, the coarse aggregate particles, mortar matrix and ITZ are modeled in 2D as separate constituents. Initially, the coarse aggregate particles are generated and placed within the domain of the sample using the “take-and-place” method proposed by Wriggers and Moftah (2006). Then, the FE mesh is generated and a mesh fragmentation procedure is applied to represent the ITZ and to define all the potential crack paths. The model is completed by adopting a tension damage model to describe the initiation and propagation of cracks under quasi-static loading.

The main characteristics of this mesoscale model are: (i) the ITZ is modeled explicitly by the use of interface elements with a high aspect ratio and its mechanical properties can be defined separately; (ii) the use of fine meshes is not necessary to describe the ITZ; (iii) multiple arbitrary cracks can be simulated without the need of tracking algorithms; and (iv) the model is developed entirely in the continuum framework, composed of standard finite elements, usually available in FEM codes, and continuum constitutive models.

2.1. Modeling of coarse aggregate

For the sake of simplicity, coarse aggregate particles are geometrically represented by regular octagons. The efficient “take-and-place” method proposed by Wriggers and Moftah (2006) is employed to generate the aggregate sizes from a grading curve, and to locate each particle in the mortar matrix randomly, so that intersection between aggregates is avoided. In addition, the grading curve may be constructed based on an experimental sieving process. Thus, for an interval $[d_s, d_{s+1}]$ defined by two sequential sieve opening sizes, d_s and d_{s+1}, the passing percentage is defined

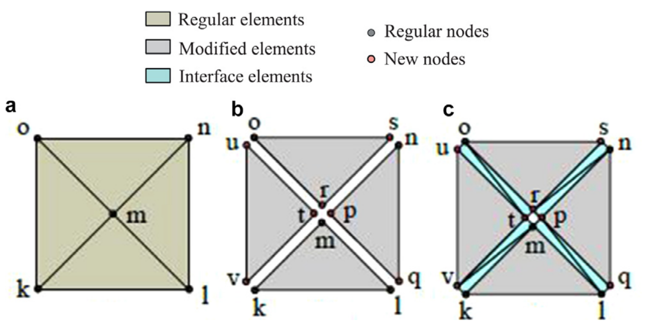

Fig. 1. Mesh fragmentation technique: (a) generation of the standard FE mesh to be fragmented, (b) separation of the finite elements by introducing gaps in between them, and (c) insertion of pairs of interface elements.

according to the equation:

$$V_p[d_s, d_{s+1}] = \frac{P(d_{s+1}) - P(d_s)}{P(d_{max}) - P(d_{min})} . V_{agg} \tag{1}$$

where d_{min} and d_{max} are the minimum and maximum particle sizes, respectively, and V_{agg} is the total volume fraction of coarse aggregate particles assumed for the concrete. It is important to note that, within this interval, the diameter of the aggregate can be defined randomly, assuming values between d_s and d_{s+1}.

Alternatively, the grading of aggregate particles may be defined by the Fuller curve, which gives an optimal packing of aggregates. The Fuller curve can be expressed by the following equation:

$$P_i = 100\left(\frac{d_i}{d_{max}}\right)^n \tag{2}$$

where P_i and d_i are the percent passing and opening size of the ith sieve, respectively, d_{max} is the maximum particle size and the exponent n assumes value between 0.45 and 0.70.

2.2. The fracture representation in the mortar matrix and ITZ

The most important step in the development of the approach proposed is the application of a mesh fragmentation technique. This technique is based on the use of standard low-order solid finite elements with a high aspect ratio to describe discontinuity by means of a continuum constitutive relation, as recently proposed by Manzoli et al. (2012). Thus, these interface elements are used in this work to represent the ITZ and to define all potential crack paths.

Fig. 1 illustrates the main steps of the mesh fragmentation technique. First, a regular (initial) FE mesh is generated (Fig. 1(a)). Then, the finite elements are separated by duplicating the common nodes and reducing their sizes, so that very narrow gaps are created between the modified regular elements (Fig. 1(b)). Finally, to fill these very thin gaps, pairs of three-node triangular elements with a high aspect ratio are inserted (Fig. 1(c)).

Note that for this simple example, in which the original mesh is composed of four three-node triangular finite elements and five nodes (see Fig. 1(a)), the fragmentation procedure requires the addition of seven extras nodes (p, q, r, s, t, u and v), as can be seen in Fig. 1(b). Hence, eight interface elements are inserted: $IE_1 = \{m, l, p\}$, $IE_2 = \{p, l, q\}$, $IE_3 = \{p, n, r\}$, $IE_4 = \{r, n, s\}$, $IE_5 = \{r, o, t\}$, $IE_6 = \{t, o, u\}$, $IE_7 = \{t, v, m\}$ and $IE_8 = \{m, v, k\}$, as can be observed in Fig. 1(c). Also note that the interface elements are defined based on the nodes of the modified regular elements and their thickness are with an exaggerated scale factor for clarity. Usually, a very small thickness (approximately 0.01 mm) is adopted.

Concrete with normal strength is assumed for the problems addressed in this paper. Hence, only the FE mesh of the mortar matrix and ITZ are fragmented, as illustrated in the Fig. 2 for a sample with one coarse aggregate particle. Note in this figure that distinct material models can be easily used to describe the failure behavior of the ITZ and the fracture process in the mortar matrix.

3. Interface solid finite element

The interface solid finite element proposed by Manzoli et al. (2012) corresponds to a standard three-node triangular finite element with a height h tending to zero ($h \to 0$), as depicted in Fig. 3. Thus, to understand the behavior of this element, it is appropriate to divide the FE approximation of the strain field, $\boldsymbol{\varepsilon}$, as follows (Manzoli et al., 2012):

$$\boldsymbol{\varepsilon} = \tilde{\boldsymbol{\varepsilon}} + \hat{\boldsymbol{\varepsilon}} = \tilde{\boldsymbol{\varepsilon}} + \underbrace{\frac{1}{h}(\mathbf{n} \otimes [\![\mathbf{u}]\!])^S}_{\hat{\boldsymbol{\varepsilon}}} \tag{3}$$

where $\hat{\boldsymbol{\varepsilon}}$ collects the components that depend on the height h, and $\tilde{\boldsymbol{\varepsilon}}$ contains the rest of the components. The notation $(\bullet)^S$ refers to the symmetric part of $(\bullet)$, $\otimes$ denotes a dyadic product, $\mathbf{n}$ is the unit vector normal to the element base and $[[\mathbf{u}]]$ is a vector that contains the components of the relative displacement between the node (1) and its projection on the element base (1′).

Note that, in the Eq. (3), when h tends to zero, the component $\tilde{\boldsymbol{\varepsilon}}$ remains bounded, while the $\hat{\boldsymbol{\varepsilon}}$ component is no longer bounded. As a consequence, the element strains are related almost exclusively

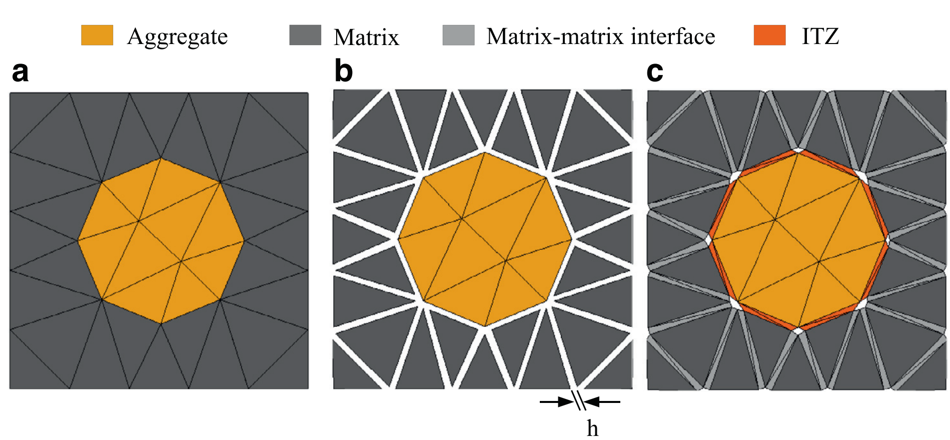

Fig. 2. Mesh fragmentation technique for a sample with one embedded aggregate: (a) original mesh, (b) introduction of gaps between all the matrix–matrix and matrix-aggregate (ITZ) elements, and (c) insertion of interface elements.

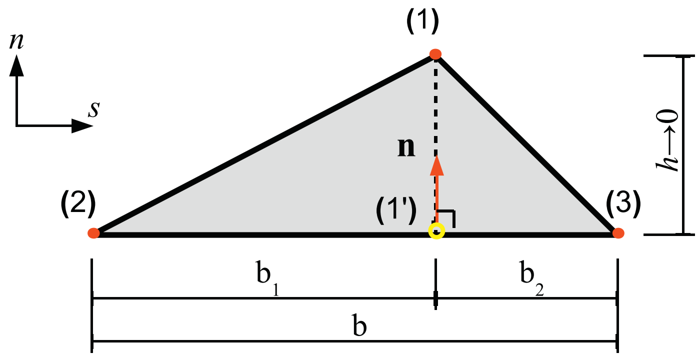

Fig. 3. Triangular interface finite element with a high aspect ratio.

to the relative displacement $[[\mathbf{u}]]$, which becomes the measure of a displacement discontinuity (strong discontinuity), and the structure of the strain field in Eq. (3) corresponds to the typical kinematics of the Continuum Strong Discontinuity Approach (CSDA). Details regarding the equivalence between the strain field of the interface finite elements and the strong discontinuity kinematics can be found in Manzoli et al. (2012).

Therefore, based on the same concepts of the CSDA, it can be stated that bounded stress can be obtained from unbounded strains by means of a continuum constitutive relation. In the following section, the continuum tension damage model used to describe the behavior of the interface elements is described.

4. Tension damage model

A constitutive model based on the Continuum Damage Mechanics Theory (CDMT) is used to describe the complex phenomenon of crack initiation and propagation through the interface solid finite elements. The formulation of this model is based on the effective stress field associated with a scalar damage variable, which varies from $d = 0$ (undamaged material) to $d = 1$ (totally damaged material). The damage criterion is based on the component of the stress component normal to the base of the element, $\bar{\sigma}_{nn}$. The damage variable degrades all the components of the effective stress tensor ($\bar{\boldsymbol{\sigma}}$) to calculate the nominal stress tensor ($\boldsymbol{\sigma}$). Thus, the proposed model is able to describe the crack propagation process controlled by a prevalent mode I.

Table 1 summarizes all the equations of the tension damage model, where $\boldsymbol{C}$ is the fourth order elastic tensor, $\boldsymbol{\varepsilon}$ is the strain tensor, r is the strain-like internal variable, f_t is the material tensile strength, h is the element's thickness and A is the softening parameter, which is related to the fracture energy G_f. More details regarding the relation between the continuum and discrete constitutive equations, in the context of CSDA, can be found in Manzoli et al. (2016).

4.1. IMPL-EX Integration scheme

To increase the stability and the robustness of the solution strategy, the IMPL-EX integration scheme proposed by Oliver et al. (2006) is used to integrate the tension damage model. Recently, this scheme has been used in several types of applications, for example for elastoplasticity problems (Oliver et al., 2008; Prazeres et al., 2016) and those described by damage mechanics (Oliver et al., 2008). The idea behind of this strategy is to combine the stability offered by explicit methods with the precision of the implicit ones. The result is the guarantee of convergence with only one iteration per load step and the positive definite character of the algorithmic tangent operator. Despite its large advantages from computational point of view, there is an error associated to the use of this integration scheme, which can be reduced (or controlled) by decreasing the load step length.

Table 1
Equations of the tension damage model.

Effective stresses	$\bar{\boldsymbol{\sigma}} = \boldsymbol{C} : \boldsymbol{\varepsilon}$
Equivalent stress	$\bar{\tau} = \bar{\sigma}_{nn}$
Damage criterion	$\bar{\phi} = \bar{\tau} - r$
Evolution law for the strain-type variable	$r(t) = \max\limits_{s\in[0,t]}[\bar{\sigma}_{nn}(s), f_t]$
Damage evolution	$d(r) = 1 - \frac{f_t}{r} e^{Ah\left(1-\frac{r}{f_t}\right)}$
Constitutive relation	$\boldsymbol{\sigma} = (1-d)\bar{\boldsymbol{\sigma}}$

Fig. 4 shows a flowchart detailing the integration of the tension damage model at the current pseudo-time t_{n+1}, which can be briefly described by the following steps:

1. Evaluate the effective stress tensor $\bar{\boldsymbol{\sigma}}_{(n+1)}$;
2. Implicit computation of the internal strain-like variable $r_{(n+1)}$;
3. Computes an explicit linear extrapolation of the internal strain-like variable in terms of the implicit values obtained in the previous time steps, $\tilde{r}_{(n+1)}\left(\tilde{r}_{(n)}, \tilde{r}_{(n-1)}\right)$;
4. Evaluate the damage variable as function of the extrapolated strain-like variable $d_{(n+1)}\left(\tilde{r}_{(n+1)}\right)$;
5. Compute the nominal stress tensor $\tilde{\boldsymbol{\sigma}}_{(n+1)}$;
6. Evaluate the effective algorithmic tangent operator $\tilde{\boldsymbol{C}}^{tang}_{(n+1)}$.

Note that the integration procedure is performed in a closed form, in which, from the given current strain tensor, $\boldsymbol{\varepsilon}_{n+1}$, the stress tensor, $\tilde{\boldsymbol{\sigma}}_{n+1}$, is evaluated explicitly and used to fulfill the balance equation and to compute the effective algorithmic tangent operator. The first two steps correspond to the implicit stage and the others to the explicit stage.

5. Numerical examples

The proposed mesoscale model for concrete is applied in two numerical examples. First, in order to study the effects of the aggregate parameters (size, volume fraction and distribution) on the material response, several uniaxial tension tests are performed. After, three-point bending beams are numerically analyzed and the results are compared with the experimental ones to investigate the capability of the strategy to simulate structural members.

Concrete with normal strength is assumed for all the examples. Thus, aggregate particles are described by linear elastic behavior and the material nonlinear response is given exclusively by the cracks represented by the mesh fragmentation technique. In addition, the tensile strength for the ITZs is assumed to be 50% of the tensile strength of the mortar matrix. This assumption induces crack initiation along the ITZs. A thickness of 0.01 mm was adopted for the interface finite elements used to represent both the ITZs and crack paths in the mortar matrix.

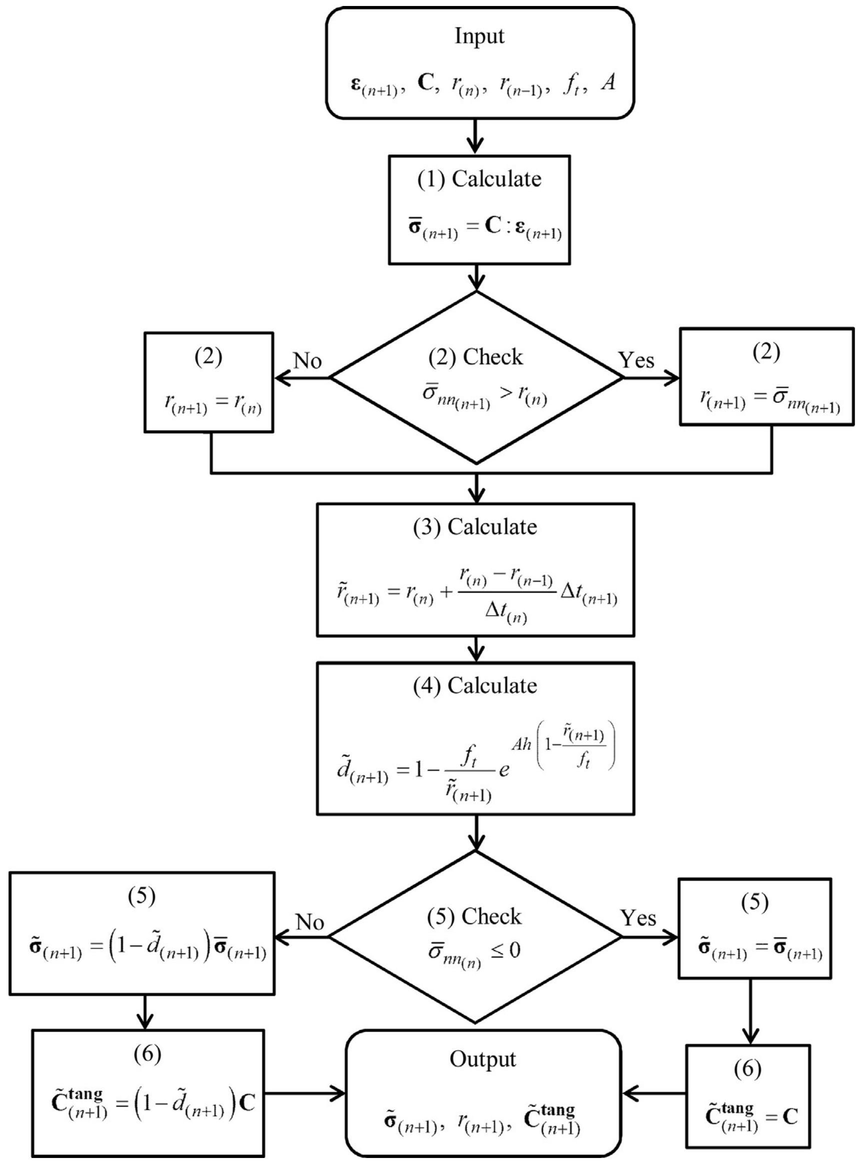

Fig. 4. Flowchart of the IMPL-EX integration scheme for the tension damage model.

5.1. Uniaxial tension tests

Several specimens with square cross section (150 mm × 150mm) under uniaxial tension load are analyzed. The analyses are performed in plane stress condition with an out-of-plane thickness of 150 mm. Fig. 5(a) shows the test setup, including the boundary conditions. As can be seen, the specimen is loaded by imposing an increasing prescribed vertical displacement along the upper face, while vertical displacements with value equal to zero are prescribed to all nodes of the lower face. The FE mesh after fragmentation procedure is depicted in Fig. 5(b). Note that interface solid elements are inserted between all the elements of the mortar matrix and between this region and the aggregate particles. However, as the ITZ is the weakest part of the material, different mechanical properties are adopted to describe the crack initiation along these thin interfaces. Following the recommendations of some authors (Huang et al., 2015; Kim and Al-Rub, 2011), the elastic modulus adopted for the ITZ is a little smaller than the mortar matrix. It is also important to mention that this small reduction has very little influence on the mechanical response of the interface element, as can be seen in Manzoli et al. (2016). The parameters adopted for each phase of the material are summarized in Table 2.

In the following sections, the effects of size, volume fraction and distribution of coarse aggregate particles on the failure process of concrete under tension are investigated. For all these cases studied, the particles are generated and placed randomly within the specimen using the method described in Section 2.1. For all of them, Fuller's grading curve is employed with $n = 0.45$.

5.1.1. Effect of aggregate size

As a first case of study, four specimens were simulated for maximum aggregate diameter of 10, 20, 30 and 40 mm, maintaining a constant aggregate volume fraction of 40% and minimum aggregate diameter of 4.75 mm.

The vertical normal stress and crack propagation process for the case with maximum aggregate diameter of 30 mm are illustrated in Fig. 6, which can be better understood with the aid of the graph plotted in Fig. 7. Thus, a first load stage can be characterized by a linear elastic response, until about 60% of the peak-load (Fig. 7– stage I), and where no damage is observed in the sample

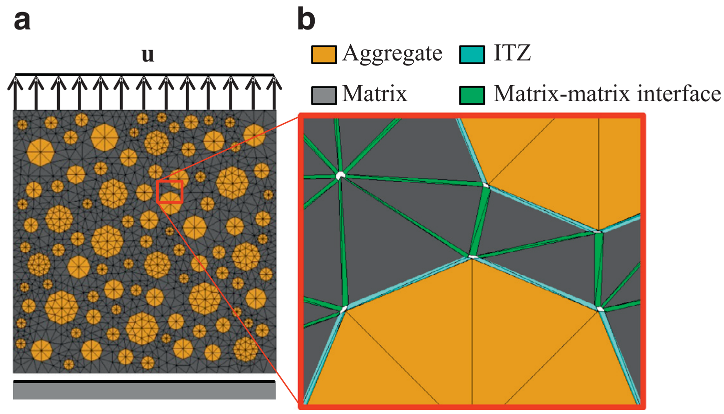

Fig. 5. Specimen under tension load: (a) geometry and boundary condition and (b) close-up showing the details of the fragmented mesh.

Table 2
Material parameters for the uniaxial tension tests.

Materials	Elastic modulus	Poisson's ratio	Fracture energy	Tensile strength
Coarse aggregate	$E_{agg} = 37.0\,\text{GPa}$	$\nu_{agg} = 0.2$	–	–
Mortar matrix	$E_m = 20.0\,\text{GPa}$	$\nu_m = 0.2$	–	–
Matrix–matrix interface	$E_{mi} = 20.0\,\text{GPa}$	$\nu_{mi} = 0$	$G_{f_{mi}} = 0.03\,\text{N/mm}$	$f_{t_{mi}} = 2.6\,\text{MPa}$
ITZ	$E_{itz} = 18.0\,\text{GPa}$	$\nu_{itz} = 0$	$G_{f_{itz}} = 0.02\,\text{N/mm}$	$f_{t_{itz}} = 1.3\,\text{MPa}$

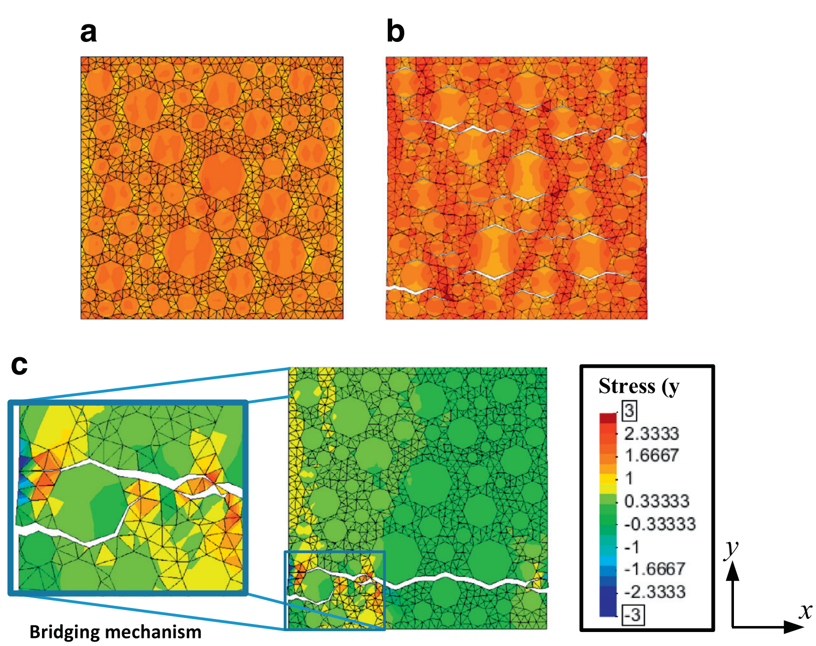

Fig. 6. Vertical normal stress and crack pattern for the case with maximum aggregate diameter of 30 mm: (a) stage I: non-damaged material (scaling factor of 300), (b) stage II: microcracks at the ITZs (scaling factor of 300) and (c) stage III: macrocrack formation due to the microcracks coalescence (scaling factor of 50).

(Fig. 6(a)). Above this load, the damage starts and a number of microcracks are simultaneously formed, predominantly perpendicular to the load direction at the ITZs, as can be seen in Fig. 6(b). In the structural response, this distributed damage configuration represents the transition from the linear to nonlinear regime before the peak-load (Fig. 7– stage II). Then, with increasing load, some microcracks propagate through the mortar matrix, while at the same time, others are being unloaded or even closed. At this final stage, the microcracks coalesce resulting in a predominant crack located at a narrow region of the specimen (Fig. 6(c)), corresponding to the softening behavior of the structural curve (Fig. 7– stage III).

The bridging mechanisms between cracks observed in experiments (van Mier, 1991; 1997) could also be observed in the numerical results (see detail of the Fig. 6(c)), where the aggregate or part of the matrix is superimposed by cracking (interlocking aggregate or overlapping crack segments), transmitting loading between their faces and contributing to residual force exhibited in the curve depicted in Fig. 7. Moreover, the superposition of cracks may be responsible for a significant increase of the fracture energy, since the bridging mechanism may remain active during the macrocrack propagation and can contribute significantly to the deviation of the macrocrack formation, consequently increasing the fracture surface area, as already reported in previous works (Landis and Bolander, 2009; van Mier and Nooru-Mohamed, 1990).

Final crack patterns for the four cases studied are shown in Fig. 8. As can be seen in this figure, the crack pattern depends

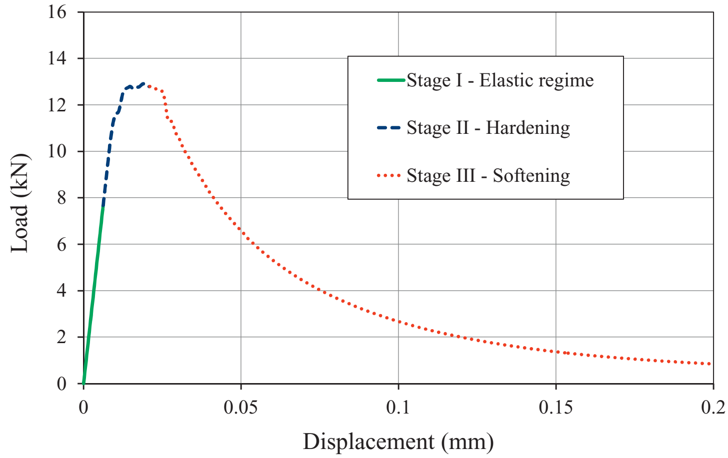

Fig. 7. Different stages of load-displacement response for the specimen with maximum aggregate diameter of 30 mm.

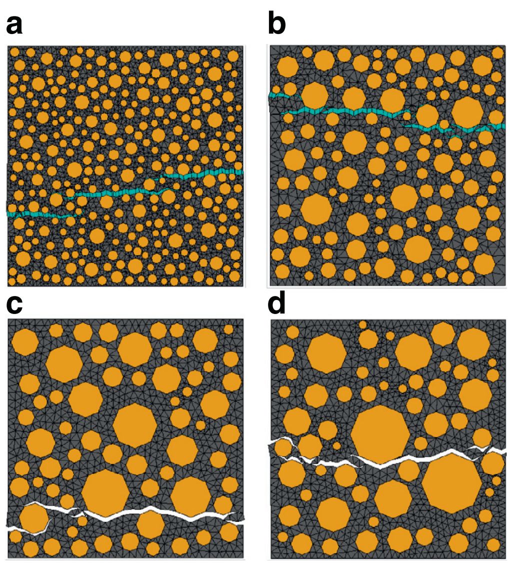

Fig. 8. Final crack patterns obtained for different maximum aggregate diameters: (a) $d = 10$ mm (showing the IE), (b) $d = 20$ mm (showing the IE), (c) $d = 30$ mm (without showing the IE) and (d) $d = 40$ mm (without showing the IE). (figures with a scaling factor of 50).

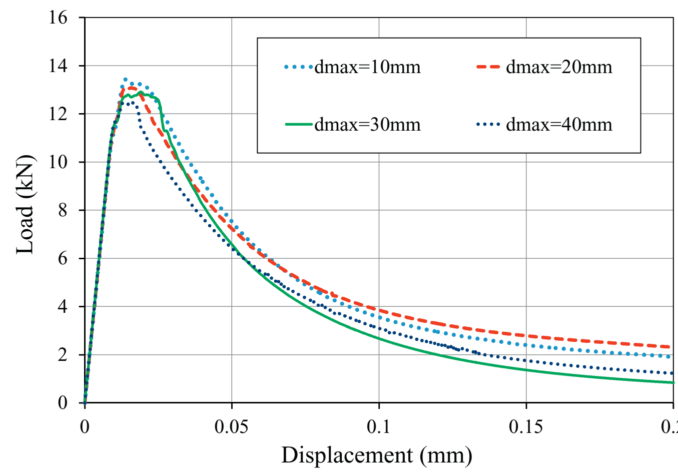

Fig. 9. Load-displacement curves for the four specimens with maximum aggregate diameter of 10, 20, 30 and 40 mm.

on the aggregate size. This effect becomes clear by observing the graphs in Fig. 9, in which it can be noted that increasing the aggregate size leads to a significant peak resistance reduction and a pronounced variation of the amount of dissipated energy for the same aggregate volume fraction. The less pronounced softening branch shown can be explained by the bridging or other form of crack face interaction that tends to increase the residual strength and, consequently, the area under the curve and so also the dissipated energy. These same qualitative and quantitative behaviors have been observed by some authors in numerical studies (Du et al., 2014; Kim and Al-Rub, 2011; López et al., 2008) and experimental investigations, for samples subjected to direct tension (Hordijk, 1992) or three-point bending tests (Zhang et al., 2010).

To clearly illustrate the detailed crack initiation and propagation processes, the deformed meshes of the specimens are showed in Fig. 6 by adopting different scaling factors. Furthermore, the interface solid elements may or may not be shown in the post-process, as illustrated in Fig. 8(a) and (b), showing the deformed interface elements, or in Fig. 8(c) and (d), without showing them. However, in the remainder of this work the interface elements are no longer shown since the crack paths are clearer without them.

5.1.2. Effect of aggregate volume fraction

Specimens with coarse aggregate volume fractions of 20, 30, 40 and 50% were numerically simulated for the same aggregate gradation (aggregate diameter varying the between $d_{min} = 5$ mm and $d_{max} = 10$ mm). The results obtained in terms of crack patterns are depicted in Fig. 10 and their corresponding load-displacement curves are plotted in Fig. 11. As shown, the crack paths for the four cases are distinct. A lower aggregate volume fraction leads to a higher peak-load. Similar results were obtained in previous numerical studies (Kim and Al-Rub, 2011; López et al., 2008; Wang et al., 2015).

Since the behavior of the coarse aggregates is described by a linear elastic response, the results obtained consolidate the fact that the ITZ plays a very important role in the concrete structural behavior under tension load. As reported by Landis and Bolander (2009), a high percentage of aggregate can induce coupling between interfaces, forming paths conducive to the formation of crack (percolation of interfaces zones) which can contribute to reducing the tensile strength of concrete.

5.1.3. Effect of aggregate distribution

Four random generations of aggregates are performed to study the effect of aggregate distribution for a constant volume fraction

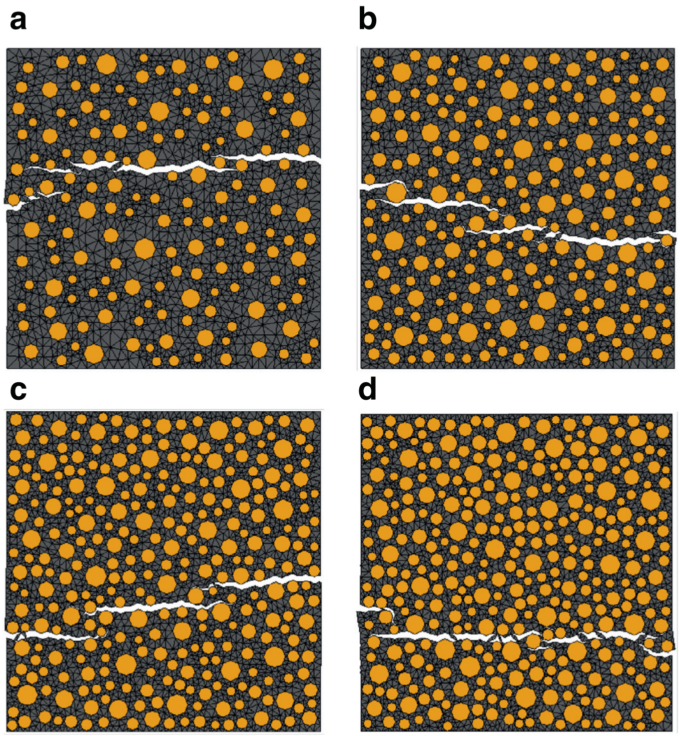

Fig. 10. Final crack patterns for different aggregate volume fractions: (a) $V_{agg} = 20\%$, (b) $V_{agg} = 30\%$, (c) $V_{agg} = 40\%$ and (d) $V_{agg} = 50\%$ (scaling factor of 50).

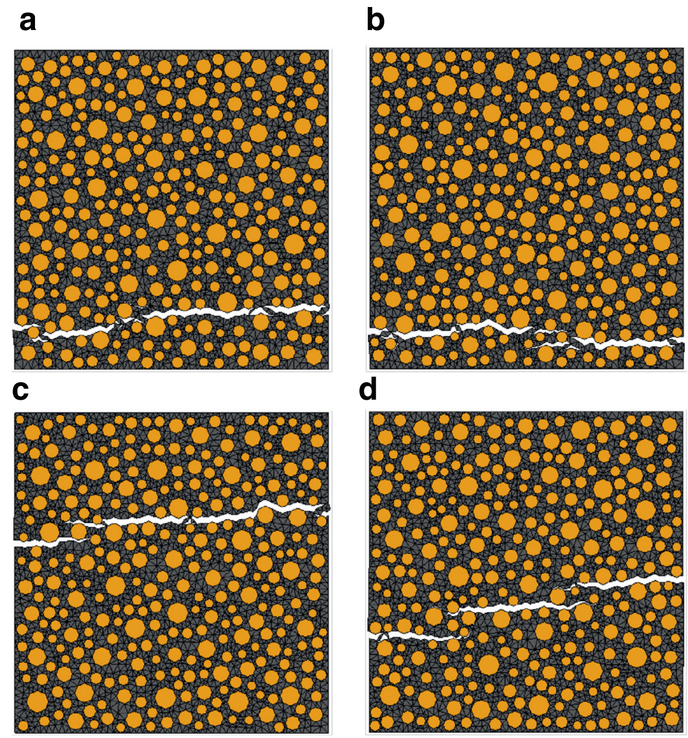

Fig. 12. Final crack patterns for different random realizations of coarse aggregate: (a) realization 1, (b) realization 2, (c) realization 3 and (d) realization 4 (scaling factor of 50).

of aggregate equal to 40% and for the same aggregate gradation with minimum and maximum diameter of aggregate equal to $d_{min} = 5\,\text{mm}$ and $d_{max} = 10\,\text{mm}$, respectively. As expected, the final crack patterns obtained for the four cases are distinct, as can be seen in Fig. 12. Furthermore, it is possible to note in the load-displacement curves illustrated in Fig. 13 that the randomly aggregate distribution affects only the post-peak structural response of the numerical simulations. Thus, it is reasonable to state that for this case study, the aggregate distribution has a negligible influence on the mechanical properties of concrete until the peak-load. Furthermore, the slightly different softening branches can be justified by the distinct crack paths obtained (see Fig. 12). According to Tejchman and Bobiński (2013), this may explain the difficulty in finding a representative volume for random heterogeneous material like concrete, for which the process zone of strain localization occurs at the weakest zone, which is dependent on their constituent material arrangements.

The results obtained in these numerical simulations are in good agreement with those obtained by other researchers (Kim and Al-Rub, 2011; Wang et al., 2015).

5.2. Three-point bending tests

A series of three-point bending tests were experimentally performed by Grégoire et al. (2013). In that research, notched and unnotched beams with different length/depth ratio for a constant out-of-plane thickness of 50mm were tested in order to study size effect. The experimental tests were carried out applying a quasi-static vertical loading at the top of the beams and by controlling

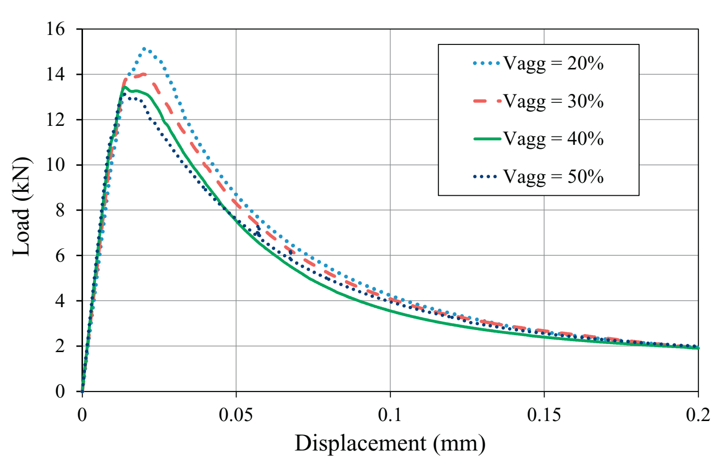

Fig. 11. Load-displacement curves for the specimens with different aggregate volume fractions.

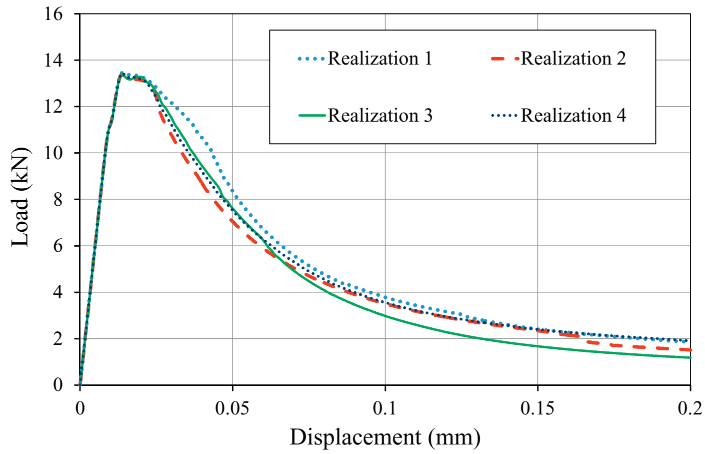

Fig. 13. Load-displacement curves for the specimens with different random realizations of coarse aggregate.

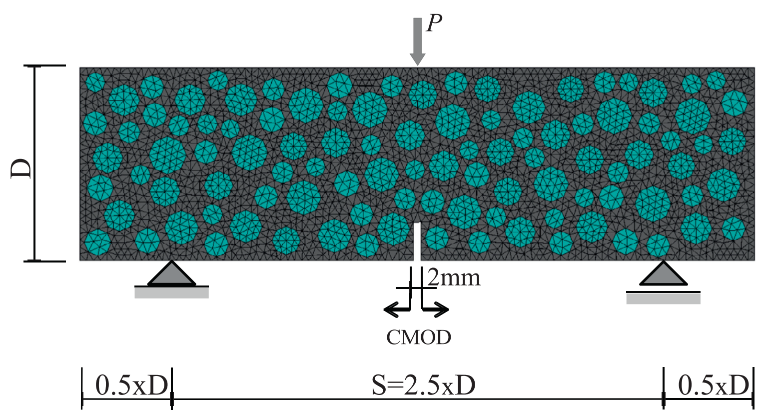

Fig. 14. Geometry, boundary conditions and FE mesh of the beam B1.

Table 3
Material parameters for the beams.

Materials	Young's modulus	Poisson's ratio	Fracture energy	Tensile strength
Coarse aggregate	$E_{agg} = 50.0\,\text{GPa}$	$\nu_{agg} = 0.2$	–	–
Mortar matrix	$E_m = 30.2\,\text{GPa}$	$\nu_m = 0.2$	–	–
Matrix–matrix interface	$E_{mi} = 30.2\,\text{GPa}$	$\nu_{mi} = 0$	$G_{f_{mi}} = 0.1\,\text{N/mm}$	$f_{t_{mi}} = 5.2\,\text{MPa}$
ITZ	$E_{itz} = 30.2\,\text{GPa}$	$\nu_{itz} = 0$	$G_{f_{itz}} = 0.05\,\text{N/mm}$	$f_{t_{itz}} = 2.6\,\text{MPa}$

the crack mouth opening displacement (CMOD) at the bottom, as illustrated in Fig. 14.

The so-called fifth-notched beams (with notch-to-depth ratio of 0.2) are chosen to be numerically analyzed with the proposed mesoscale approach. The beams of this group are classified according to their depth as: B1 ($D = 50\,\text{mm}$), B2 ($D = 100\,\text{mm}$), B3 ($D = 200\,\text{mm}$) and B4 ($D = 400\,\text{mm}$), from smallest to largest beam size. Fig. 14 shows the standard geometry, boundary conditions and the FE mesh adopted for the beam B1. As can be seen in this figure, the entire domain of the problem is discretized by generating computational models with 16,017; 27,174; 107,779 and 428,709 finite elements for the corresponding four beam sizes.

The aggregate particles are placed into the mortar matrix one by one randomly, using the experimental particle size distribution provided by Grégoire et al. (2013) and illustrated in Fig. 15, considering a volume fraction of 40% and varying the aggregate diameter from $d_{min} = 5\,\text{mm}$ to $d_{max} = 10\,\text{mm}$.

The material properties adopted for each constituent of the mesoscale models are listed in Table 3. However, it is important to mention that only Young's modulus of concrete ($E_c = 37\text{GPa}$) was provided by the experiments. Thereby, adopting a Young's modulus of aggregate equals to $E_{agg} = 50\,\text{GPa}$, Young's modulus of mortar matrix was predicted using an inverse analysis based on the rule of mixture, as proposed by Counto (1964). Then, the same value was adopted for Young's modulus of the interface elements.

The tensile strength of the matrix–matrix interface elements and for the interface elements of the ITZ were calculated, so that the average value is equivalent to that obtained experimentally by Grégoire et al. (2013) for the concrete (mean value of 3.9 MPa obtained by the splitting tensile test of standard cylinders experimentally analyzed), with a ratio between them of 2, i.e. $f_{t_{mi}}/f_{t_{itz}} = 2$. In addition, the same strategy were applied for the fracture energy parameters, $\left(G_{f_{mi}} + G_{f_{itz}}\right)/2 = G_C$, keeping $G_{f_{mi}}/G_{f_{itz}} = 2$, where G_C is the concrete fracture energy and its assumed value is 0.075 N/mm, similar to that chosen numerically by Grassl et al. (2012) (see Table 3).

The numerical analyses are carried out applying an incremental vertical load at the top mid-point of the beams using the displacement control method, controlling the vertical displacement of the point where the load is applied.

Fig. 16 shows the crack pattern obtained for the four beams. As expected, the strains are practically all concentrated in those

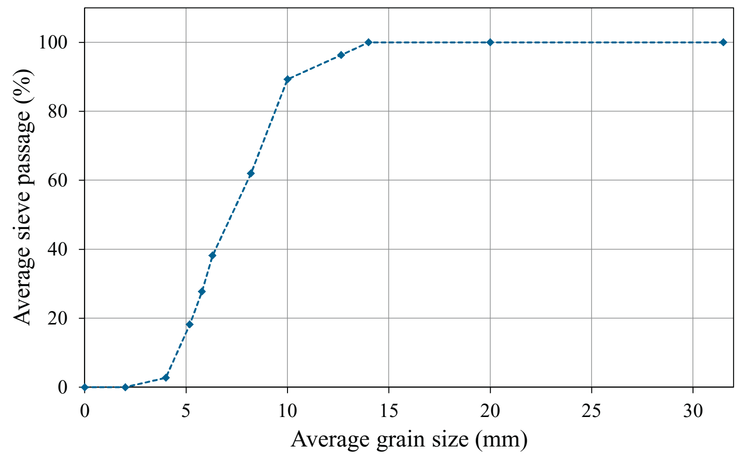

Fig. 15. Experimental grading curve of aggregate provided by Grégoire et al. (2013).

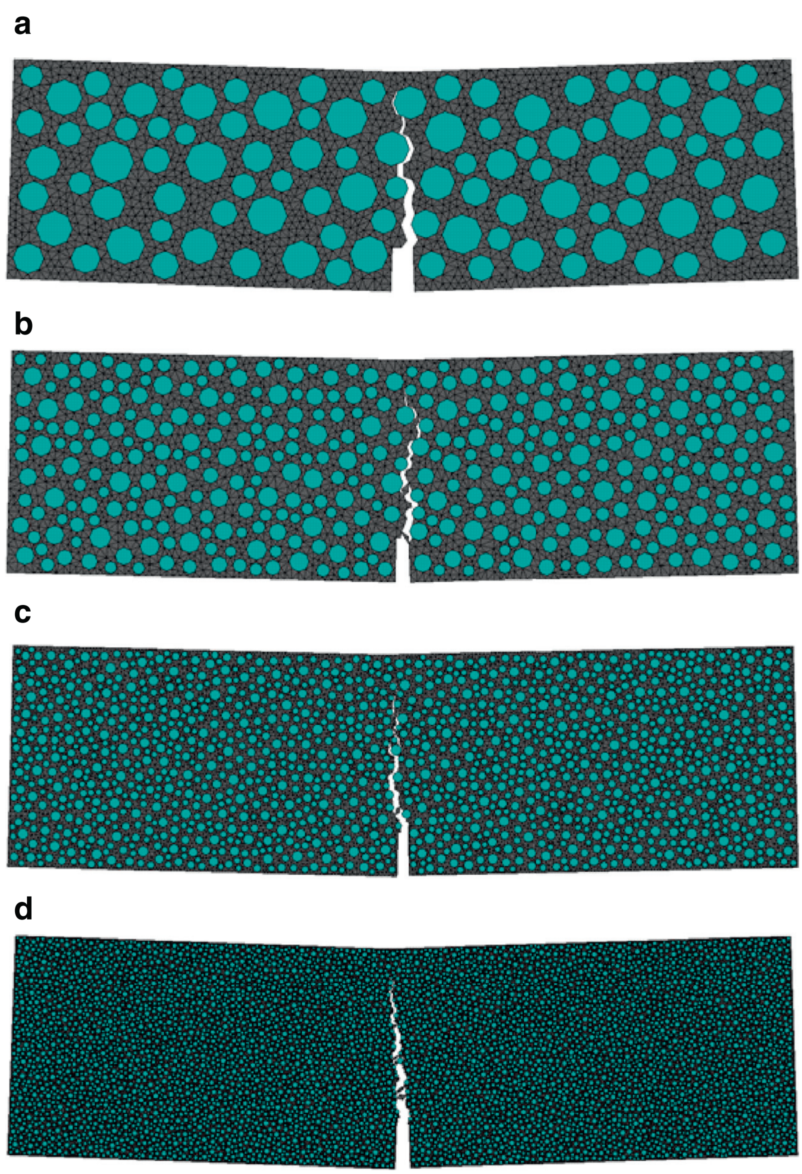

Fig. 16. Numerical crack patterns obtained for the beams: (a) B1, (b) B2, (c) B3 and (d) B4.

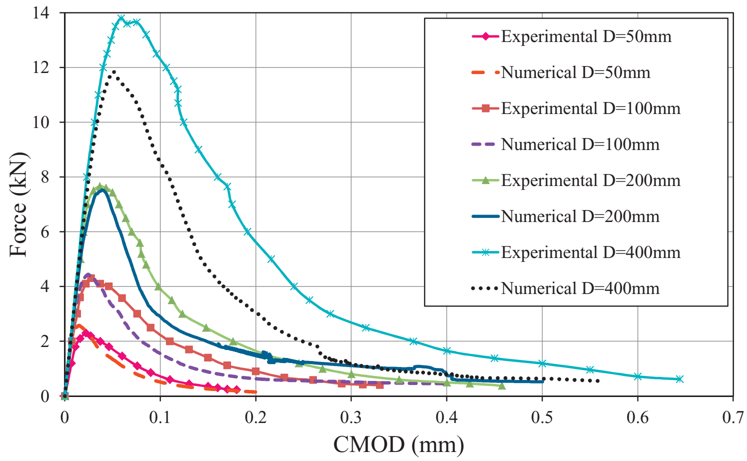

Fig. 17. Comparison between numerical and experimental results: Force-CMOD curves.

interface elements near of the central cross section, following a dominant vertical crack propagation (in mode I) from the notch, with a zigzag path induced by the weakest ITZ and imposed by the FE mesh of the mortar matrix.

Note that, although the crack patterns are very similar for the four cases analyzed, the aggregate distribution directly influences the crack path. The same observation was reported by other references (Grégoire et al., 2013; Hordijk, 1992; Zhang et al., 2010). It is also important to note that the geometry of the notch was defined before the generation of the aggregates (see Fig. 16), which would be equivalent to a cast-in notch. The results would have been more realistic if the notch had gone through the aggregates.

The numerical load-CMOD curves are compared with those obtained experimentally by Grégoire et al. (2013). As shown in Fig. 17, the numerical and experimental results are in good agreement for the beams B1, B2 and B3, while the numerical result obtained for the beam B4, underestimates the peak-load and the softening branch. However, it is important to note in the graphs that the numerical model is capable of representing the size effect. The results present the same tendency described in previous works (Grassl et al., 2012; Grégoire et al., 2013; Skarżyński and Tejchman, 2010), in which the peak load increases and the softening branches become more pronounced as the beam size increases.

6. Summary and conclusions

This paper presents an alternative 2D mesoscale model, in which the concrete is considered as a heterogeneous three-phase material composed of coarse aggregates, mortar matrix and ITZ. The main novelty of the proposed approach is the use of interface solid finite elements developed by Manzoli et al. (2012) to represent the complex ITZ and crack propagation process based on a mesh fragmentation technique (Manzoli et al., 2016).

The shape of the coarse aggregates was represented by regular octagons and an efficient "take-and-place" method, proposed by Wriggers and Moftah (2006), was used to generate and randomly place the aggregates within the sample. This technique is very appealing since the aggregate size can be generated from an grading curve. Studies including irregular aggregate could lead to interesting results and this issue will be addressed in a future paper.

First, several uniaxial tension tests were numerically analyzed in order to study the effects of aggregate parameters, such as size, volume fraction and its distribution, on the tensile strength and dissipated energy. In general, the mechanical response and crack patterns were shown to be sensitive to the variation of these parameters. By increasing the maximum aggregate size, the peak load is reduced and the dissipated energy decreases. When the volume fraction increases the peak load also decreases and, regarding the load *x* displacement curves, the results were similar until the peak load, followed by different softening branches that tend to converge to a fixed residual strength.

Then, to investigate the capability of the strategy to simulate structural members, three-point bending beams were numerically analyzed and the results were compared with the experimental ones obtained by Grégoire et al. (2013). The results demonstrated that the mesoscale model was able to predict the size effect phenomenon. Moreover, for the four geometrically similar notched beams, the numerical results were in good agreement with those obtained experimentally.

The results showed that the proposed model presents the same kinds of characteristics that real 3D concrete shows, predicting the macroscopic response of concrete, considering the effects of coarse aggregate, mortar matrix and ITZ individually. It is important to note that the strategy was formulated integrally in the framework of the continuum mechanics and multiple arbitrary cracks could be simulated without the need of a tracking algorithm. In addition, the introduction of this technique to existing FE code is very simple, since only a few implementations in the pre-process stage, related to the mesh fragmentation technique, are necessary.

In future works the authors intend to extend the formulation presented here to 3D, in which the main challenge is the computational effort necessary to solve this type of problem, since the 3D mesh fragmentation technique could increase dramatically the number of finite elements. Thus, multiscale analysis based on the use of coupling finite elements (Bitencourt Jr. et al., 2015) will also be addressed.

Acknowledgments

The authors wish to acknowledge the financial support of the National Council for Scientific and Technological Development (CNPq), Coordination for the Improvement of Higher Education Personnel (CAPES) and Sao Paulo Research Foundation (FAPESP).

References

Bazant, Z.P., Tabbara, M.R., Kazemi, M.T., Pijaudier-Cabot, G., 1990. Random particle model for fracture of aggregate or fiber composites. J. Eng. Mech. 116 (8), 1686–1705. doi:10.1061/(ASCE)0733-9399(1990)116:8(1686).

Bitencourt Jr., L.A.G., Manzoli, O.L., Prazeres, P.G.C., Rodrigues, E.A., Bittencourt, T.N., 2015. A coupling technique for non-matching finite element meshes. Comput. Methods Appl. Mech. Eng. 290, 19–44. http://dx.doi.org/10.1016/j.cma.2015.02.025. http://www.sciencedirect.com/science/article/pii/S0045782515000870.

Bolander Jr., J.E., Saito, S., 1998. Fracture analyses using spring networks with random geometry. Eng. Fract. Mech. 61 (5-6), 569–591. http://dx.doi.org/10.1016/S0013-7944(98)00069-1. http://www.sciencedirect.com/science/article/pii/S0013794498000691.

Caballero, A., Carol, I., López, C., 2007. 3D meso-mechanical analysis of concrete specimens under biaxial loading. Fatigue Fract. Eng. Mater. Struct. 30 (9), 877–886. doi:10.1111/j.1460-2695.2007.01161.x.

Caballero, A., López, C., Carol, I., 2006. 3D meso-structural analysis of concrete specimens under uniaxial tension. Comput. Methods Appl. Mech. Eng. 195 (52), 7182–7195. http://dx.doi.org/10.1016/j.cma.2005.05.052.Computational Modelling of Concrete, http://www.sciencedirect.com/science/article/pii/S0045782505004068.

Carol, I., López, C., Roa, O., 2001. Micromechanical analysis of quasi-brittle materials using fracture-based interface elements. Int. J. Numer. Methods Eng. 52 (1-2), 193–215. doi:10.1002/nme.277.

Carpinteri, A., Cornetti, P., Puzzi, S., 2004. A stereological analysis of aggregate grading and size effect on concrete tensile strength. Int. J. Fract. 128 (1–4), 233–242. doi:10.1023/B:FRAC.0000040986.00333.86.

Counto, U.J., 1964. The effect of the elastic modulus of the aggregate on the elastic modulus, creep and creep recovery of concrete. Mag. Concr. Res. 16 (48), 129–138.

Cusatis, G., Bažant, Z., Cedolin, L., 2006. Confinement-shear lattice CSL model for fracture propagation in concrete. Comput. Methods Appl. Mech. Eng. 195 (52), 7154–7171. http://dx.doi.org/10.1016/j.cma.2005.04.019.Computational Modelling of Concrete. http://www.sciencedirect.com/science/article/pii/S0045782505003956.

Cusatis, G., Mencarelli, A., Pelessone, D., Baylot, J., 2011. Lattice discrete particle model (LDPM) for failure behavior of concrete. II: Calibration and validation. Cem. Concr. Compos. 33 (9), 891–905. http://dx.doi.org/10.1016/j.cemconcomp.2011.02.010. http://www.sciencedirect.com/science/article/pii/S0958946511000333.

D'Addetta, G., Ramm, E., 2006. A microstructure-based simulation environment on the basis of an interface enhanced particle model. Granul. Matter 8 (3-4), 159–174. doi:10.1007/s10035-006-0004-4.

De Schutter, G., Taerwe, L., 1993. Random particle model for concrete based on Delaunay triangulation. Mater. Struct. 26 (2), 67–73. doi:10.1007/BF02472853.

Du, X., Jin, L., Ma, G., 2014. Numerical modeling tensile failure behavior of concrete at mesoscale using extended finite element method. Int. J. Damage Mech. 23 (7), 872–898. http://dx.doi.org/10.1177/1056789513516028.

Eliáš, J., Stang, H., 2012. Lattice modeling of aggregate interlocking in concrete. Int. J. Fract. 175 (1), 1–11. doi:10.1007/s10704-012-9677-3.

Garboczi, E., 2002. Three-dimensional mathematical analysis of particle shape using X-ray tomography and spherical harmonics: Application to aggregates used in concrete. Cem. Concr. Res. 32 (10), 1621–1638. http://dx.doi.org/10.1016/S0008-8846(02)00836-0. http://www.sciencedirect.com/science/article/pii/S0008884602008360.

Grassl, P., Grégoire, D., Solano, L.R., Pijaudier-Cabot, G., 2012. Meso-scale modelling of the size effect on the fracture process zone of concrete. Int. J. Solids Struct. 49 (13), 1818–1827. http://dx.doi.org/10.1016/j.ijsolstr.2012.03.023. http://www.sciencedirect.com/science/article/pii/S0020768312001175.

Grassl, P., Jirásek, M., 2010. Meso-scale approach to modelling the fracture process zone of concrete subjected to uniaxial tension. Int. J. Solids and Struct. 47 (7-8), 957–968. http://dx.doi.org/10.1016/j.ijsolstr.2009.12.010. http://www.sciencedirect.com/science/article/pii/S0020768309004752.

Grassl, P., Pearce, C., 2010. Mesoscale approach to modeling concrete subjected to thermomechanical loading. J. Eng. Mech. 136 (3), 322–328. doi:10.1061/(ASCE)0733-9399(2010)136:3(322).

Grégoire, D., Rojas-Solano, L., Pijaudier-Cabot, G., 2013. Failure and size effect for notched and unnotched concrete beams. Int. J. Numer. Anal. Methods Geomech. 37 (10), 1434–1452. doi:10.1002/nag.2180.

Häfner, S., Eckardt, S., Luther, T., Könke, C., 2006. Mesoscale modeling of concrete: Geometry and numerics. Comput. Struct. 84 (7), 450–461. http://dx.doi.org/10.1016/j.compstruc.2005.10.003. http://www.sciencedirect.com/science/article/pii/S0045794905003585.

Hordijk, D., 1992. Tensile and tensile fatigue behaviour of concrete; experiments, modeling and analyses. Heron 37 (1), 1–79.

Huang, Y., Yang, Z., Ren, W., Liu, G., Zhang, C., 2015. 3D meso-scale fracture modelling and validation of concrete based on in-situ X-ray computed tomography images using damage plasticity model. Int. J. Solids Struct. 67-68, 340–352. http://dx.doi.org/10.1016/j.ijsolstr.2015.05.002. http://www.sciencedirect.com/science/article/pii/S0020768315002127.

Kim, S.-M., Al-Rub, R.K.A., 2011. Meso-scale computational modeling of the plastic-damage response of cementitious composites. Cem. Concr. Res. 41 (3), 339–358. http://dx.doi.org/10.1016/j.cemconres.2010.12.002.

Landis, E., Bolander, J., 2009. Explicit representation of physical processes in concrete fracture. J. Phys. D Appl. Phys. 42 (21), 1–17. http://stacks.iop.org/0022-3727/42/i=21/a=214002.

Leite, J., Slowik, V., Mihashi, H., 2004. Computer simulation of fracture processes of concrete using mesolevel models of lattice structures. Cem. Concr. Res. 34 (6), 1025–1033. http://dx.doi.org/10.1016/j.cemconres.2003.11.011. http://www.sciencedirect.com/science/article/pii/S0008884603004083.

Lilliu, G., van Mier, J., 2003. 3D lattice type fracture model for concrete. Eng. Fract. Mech. 70 (7-8), 927–941. http://dx.doi.org/10.1016/S0013-7944(02)00158-3. http://www.sciencedirect.com/science/article/pii/S0013794402001583.

López, C.M., Carol, I., Aguado, A., 2008. Meso-structural study of concrete fracture using interface elements. I: numerical model and tensile behavior. Mater. Struct. 41 (3), 583–599. doi:10.1617/s11527-007-9314-1.

Manzoli, O., Gamino, A., Rodrigues, E., Claro, G., 2012. Modeling of interfaces in two-dimensional problems using solid finite elements with high aspect ratio. Comput. Struct. 94-95 (0), 70–82. doi:10.1016/j.compstruc.2011.12.001. http://www.sciencedirect.com/science/article/pii/S0045794911002938.

Manzoli, O.L., Maedo, M.A., Bitencourt Jr., L.A., Rodrigues, E.A., 2016. On the use of finite elements with a high aspect ratio for modeling cracks in quasi-brittle materials. Eng. Fract. Mech. 153, 151–170. http://dx.doi.org/10.1016/j.engfracmech.2015.12.026. http://www.sciencedirect.com/science/article/pii/S001379441500702X.

van Mier, J., 1991. Mode I fracture of concrete: Discontinuous crack growth and crack interface grain bridging. Cem. Concr. Res. 21 (1), 1–15. http://dx.doi.org/10.1016/0008-8846(91)90025-D. http://www.sciencedirect.com/science/article/pii/000888469190025D.

van Mier, J., 1997. Fracture Processes of Concrete: Assessment of Material Parameters for Fracture Models. CRC Press.

van Mier, J.G., Nooru-Mohamed, M., 1990. Geometrical and structural aspects of concrete fracture. Eng. Fract. Mech. 35 (4-5), 617–628. http://dx.doi.org/10.1016/0013-7944(90)90144-6. http://www.sciencedirect.com/science/article/pii/0013794490901446.

Mier, J.V., Vliet, M.V., 2003. Influence of microstructure of concrete on size/scale effects in tensile fracture. Eng. Fract. Mech. 70 (16), 2281–2306. http://dx.doi.org/10.1016/S0013-7944(02)00222-9.Size-scale effects, http://www.sciencedirect.com/science/article/pii/S0013794402002229.

Monteiro, P., Maso, J., Ollivier, J., 1985. The aggregate-mortar interface. Cem. Concr. Res. 15 (6), 953–958. http://dx.doi.org/10.1016/0008-8846(85)90084-5. http://www.sciencedirect.com/science/article/pii/0008884685900845.

Niknezhad, D., Raghavan, B., Bernard, F., Kamali-Bernard, S., 2015. Towards a realistic morphological model for the meso-scale mechanical and transport behavior of cementitious composites. Compos. Part B Eng. 81, 72–83. http://dx.doi.org/10.1016/j.compositesb.2015.06.024. http://www.sciencedirect.com/science/article/pii/S135983681500400X.

Oliver, J., Caicedo, M., Roubin, E., Huespe, A., Hernández, J., 2015. Continuum approach to computational multiscale modeling of propagating fracture. Comput. Methods Appl. Mech. Eng. 294, 384–427. http://dx.doi.org/10.1016/j.cma.2015.05.012. http://www.sciencedirect.com/science/article/pii/S0045782515001851.

Oliver, J., Huespe, A., Blanco, S., Linero, D., 2006. Stability and robustness issues in numerical modeling of material failure with the strong discontinuity approach. Comput. Methods Appl. Mech. Eng. 195 (52), 7093–7114.Computational Modelling of Concrete.

Oliver, J., Huespe, A., Cante, J., 2008. An implicit/explicit integration scheme to increase computability of non-linear material and contact/friction problems. Comput. Methods Appl. Mech. Eng. 197 (21–24), 1865–1889. http://dx.doi.org/10.1016/j.cma.2007.11.027. http://www.sciencedirect.com/science/article/pii/S0045782507004756.

Prazeres, P.G.C., Bitencourt Jr., L.A.G., Bittencourt, T.N., Manzoli, O.L., 2016. A modified implicit–explicit integration scheme: an application to elastoplasticity problems. J. Braz. Soc. Mech. Sci. Eng. 38 (1), 151–161. doi:10.1007/s40430-015-0343-3.

Rodrigues, E.A., Manzoli, O.L., Bitencourt Jr., L.A.G., Prazeres, P.G.C., Bittencourt, T.N., 2015. Failure behavior modeling of slender reinforced concrete columns subjected to eccentric load. Lat. Am. J. Solids Struct. 12 (3), 520–541. http://dx.doi.org/10.1590/1679-78251224.

Roubin, E., Vallade, A., Benkemoun, N., Colliat, J.-B., 2015. Multi-scale failure of heterogeneous materials: A double kinematics enhancement for embedded finite element method. Int. J. Solids Struct. 52, 180–196. http://dx.doi.org/10.1016/j.ijsolstr.2014.10.001. http://www.sciencedirect.com/science/article/pii/S0020768314003710.

Sánchez, M., Manzoli, O., Guimarães, L., 2014. Modeling 3-D desiccation soil crack networks using a mesh fragmentation technique. Comput. Geotech. 62 (0), 27–39. http://dx.doi.org/10.1016/j.compgeo.2014.06.009. http://www.sciencedirect.com/science/article/pii/S0266352X14001177.

Schlangen, E., Garboczi, E., 1997. Fracture simulations of concrete using lattice models: Computational aspects. Eng. Fract. Mech. 57 (2-3), 319–332. http://dx.doi.org/10.1016/S0013-7944(97)00010-6. http://www.sciencedirect.com/science/article/pii/S0013794497000106.

Schlangen, E., van Mier, J., 1992. Simple lattice model for numerical simulation of fracture of concrete materials and structures. Mater. Struct. 25 (9), 534–542. doi:10.1007/BF02472449.

Skarżyński, Ł., Tejchman, J., 2010. Calculations of fracture process zones on meso-scale in notched concrete beams subjected to three-point bending. Eur. J. Mech. A Solids 29 (4), 746–760. http://dx.doi.org/10.1016/j.euromechsol.2010.02.008. http://www.sciencedirect.com/science/article/pii/S0997753810000379.

Tejchman, J., Bobiński, J., 2013. Continuous and Discontinuous Modelling of Fracture in Concrete using FEM. Springer Series in Geomechanics and Geoengineering, Springer. Berlin doi:10.1007/978-3-642-28463-2.

Unger, J.F., Eckardt, S., 2011. Multiscale modeling of concrete: From mesoscale to macroscale. Arch. Comput. Methods Eng. 18 (3), 341–393. doi:10.1007/s11831-011-9063-8.

Wang, X., Yang, Z., Jivkov, A.P., 2015. Monte Carlo simulations of mesoscale fracture of concrete with random aggregates and pores: a size effect study. Constr. Build. Mater. 80, 262–272. http://dx.doi.org/10.1016/j.conbuildmat.2015.02.002. http://www.sciencedirect.com/science/article/pii/S0950061815001154.

Wang, Z., Kwan, A., Chan, H., 1999. Mesoscopic study of concrete I: Generation of random aggregate structure and finite element mesh. Comput. Struct. 70 (5), 533–544. http://dx.doi.org/10.1016/S0045-7949(98)00177-1. http://www.sciencedirect.com/science/article/pii/S0045794998001771.

Wittmann, F.H., Sadouki, H., Steiger, T., 1993. Experimental and numerical study of effective properties of composite materials. Huet, C., Micromechanics of Concrete and Cementitious Composites, Universitaires Romandes Lausanne.

de Wolski, S., Bolander, J., Landis, E., 2014. An in-situ X-ray microtomography study of split cylinder fracture in cement-based materials. Exp. Mech. 54 (7), 1227–1235. doi:10.1007/s11340-014-9875-1.

Wriggers, P., Moftah, S., 2006. Mesoscale models for concrete: Homogenisation and damage behaviour. Finite Elem. Anal. Des. 42 (7), 623–636. http://dx.doi.org/10.1016/j.finel.2005.11.008.The Seventeenth Annual Robert J. Melosh Competition. The Seventeenth Annual Robert J. Melosh Competition, http://www.sciencedirect.com/science/article/pii/S0168874X05001563.

Zhang, J., Leung, C., Xu, S., 2010. Evaluation of fracture parameters of concrete from bending test using inverse analysis approach. Mater. Struct. 43 (6), 857–874. doi:10.1617/s11527-009-9552-5.

Zubelewicz, A., Bažant, Z., 1987. Interface element modeling of fracture in aggregate composites. J. Eng. Mech. 113 (11), 1619–1630. doi:10.1061/(ASCE)0733-9399(1987)113:11(1619).